Available online at www.sciencedirect.com
ScienceDirect
Journal of Power Sources 177 (2008) 500–505
JOURNAL OF POWER SOURCES
www.elsevier.com/locate/jpowsour

Short communication

The reaction pathway and rate-limiting step of dehydrogenation of the $LiHN_2 + LiH$ mixture

Leon L. Shaw *, William Osborn, Tippawan Markmaitree, Xuefei Wan

Department of Chemical, Materials and Biomolecular Engineering, University of Connecticut, Storrs, CT, USA

Received 8 October 2007; received in revised form 8 November 2007; accepted 9 November 2007
Available online 21 November 2007

Abstract

The reaction pathway and rate-limiting step of dehydrogenation of the $LiNH_2 + LiH$ mixture have been investigated. The study reveals that dehydrogenation of the $LiNH_2 + LiH$ mixture is diffusion-controlled and the rate-limiting step is NH_3 diffusion through the Li_2NH product layer outside the $LiNH_2$ shrinking core. This phenomenon is explained based on a model describing the major steps of the dehydriding reaction of the mixture, and related to the evidence obtained from X-ray diffraction and specific surface area measurements of the mixture before and after isothermal hydrogen uptake/release cycles at high homologous temperatures.

Keywords: Hydrogen storage materials; $LiNH_2$; LiH; Reaction kinetic; Reaction mechanism

1. Introduction

Since the first report by Chen et al. [1] in 2002, studies on hydrogen sorption and desorption behavior and mechanisms of the lithium amide ($LiNH_2$) and lithium hydride (LiH) mixture have been very active [2–15]. It is generally agreed that the overall dehydriding reaction of this system is expressed as [1]:

$$LiNH_2 + LiH = Li_2NH + H_2 \quad (1)$$

This reaction can theoretically absorb and desorb 6.5 wt.% hydrogen, and its reaction heat has been calculated to be 44.5 kJ mol^{-2} H_2 [1], although a recent measurement [9] suggests that the reaction heat might be 65.6 kJ mol^{-2} H_2, higher than the previous theoretical estimation [1]. Additionally, many studies [4,5,11,16] have provided strong evidence that Reaction (1) proceeds with two elementary reactions. First, $LiNH_2$ decomposes, as shown in Reaction (2):

$$LiNH_2 = 1/2Li_2NH + 1/2NH_3 \quad (2)$$

The ammonia (NH_3) from Reaction (2) then reacts with LiH to form $LiNH_2$ again and liberate H_2, as shown in Reaction (3):

$$1/2NH_3 + 1/2LiH = 1/2LiNH_2 + 1/2H_2 \quad (3)$$

For a mixture of $LiNH_2 + LiH$ (with a molar ratio of 1:1), the reaction would continue to repeat the cycle of Reactions (2) and (3) until all $LiNH_2$ and LiH transform to lithium imide (Li_2NH) and H_2 completely.

It has been demonstrated that Reaction (3) is ultrafast and can take place in the order of microseconds [4]. In contrast, using pure $LiNH_2$ as the starting material, it has been shown that Reaction (2) is diffusion-controlled and proceeds in minutes [17]. It is interesting to note that both Reactions (2) and (3) have solid products, yet one could proceed in microseconds and the other requires much longer time to complete. The reason for such a large difference in the reaction kinetics between Reactions (2) and (3) has not been studied. The reaction kinetics of Reaction (1), i.e., the combined reaction of Reactions (2) and (3), has never been investigated either. This study has been conducted as the first attempt to investigate these issues and identify the rate-limiting step for dehydrogenation of Reaction (1). The understanding developed from this study will shed light on how to increase the dehydrogenation rate of the $LiNH_2 + LiH$ mixture.

* Corresponding author. Tel.: +1 860 486 2592; fax: +1 860 486 4745.
E-mail address: leon.shaw@uconn.edu (L.L. Shaw).

0378-7753/$ – see front matter © 2007 Elsevier B.V. All rights reserved.
doi:10.1016/j.jpowsour.2007.11.029

2. Materials and methods

Lithium amide with 95% purity was purchased from Alfa Aesar, while lithium hydride with 95% purity was purchased from Sigma–Aldrich. The $LiNH_2$ and LiH mixture was prepared with a molar ratio of 1:1.1 according to Reaction (1). The 10% excess of LiH was added to minimize the loss of NH_3 during the dehydriding process. High-energy ball milling was conducted using a modified Szegvari attritor, which had been shown previously to be effective in preventing the formation of the dead zone and producing uniform milling products within the powder charge [18]. Sample loading and subsequent ball milling were conducted under an argon atmosphere, and other ball milling conditions can be found elsewhere [16].

After ball milling for 3 h at room temperature, the $LiNH_2$ + LiH mixture was then subjected to various characterizations and handled in a glove-box filled with Ar of 99.999% purity. The characterization included (i) the specific surface area (SSA) measurement through nitrogen adsorption at 77 K based on the Brunauer–Emmett–Teller (BET) method [19] using a gas sorption analyzer (NOVA 1000), (ii) X-ray diffraction (XRD) using a D5005 ADAVANCE diffractometer with Cu Kα radiation, and (iii) an isothermal soak/release cycle using a Sieverts'-type pressure–composition–isotherm (PCI) device (Advanced Materials Corporation). Detailed experimental conditions for SSA measurement and XRD data collection can be found elsewhere [16], and thus will not be repeated here.

The isothermal soak/release cycle entailed a 1 h sorption at a hydrogen pressure of 10 atm and a subsequent 2.5 h desorption under an evacuated condition, at 285 or 240 °C and repeated for 10 times. The sorption segment in each soak/release cycle was done in one step, i.e., exposing the sample to a hydrogen pressure of 10 atm until 1 h was reached. In contrast, the desorption segment in each soak/release cycle was accomplished in 10 evacuation steps in order to maintain an evacuated condition. The sample chamber was closed for 15 min between every two consecutive evacuation steps in order to quantify how much hydrogen was released in the next evacuation step. During each 15 min holding, the pressure of the sample chamber increased gradually because of desorption of hydrogen from the sample and was recorded to calculate the hydrogen desorbed as a function of time. The sum of the hydrogen desorbed in 10 evacuation steps represented the total amount of hydrogen desorbed from the sample in one release cycle which lasted 2.5 h (i.e., 15 min per holding × 10 steps). The pressure of the sample chamber was less than 0.003 atm at the end of the 10th holding step. Thus, the total amount of hydrogen desorbed in one release cycle could be regarded approximately as the amount of hydrogen released in 2.5 h under a constant temperature (e.g., 285 °C) and a constant hydrogen pressure (i.e., 0.003 atm).

3. Results and discussion

Shown in Fig. 1 are the absorbed and desorbed hydrogen (in wt.%) of the $LiNH_2$ + LiH mixture during isothermal soak/release cycles at 285 °C. It is clear that the mixture has a rapid hydrogen sorption rate (i.e., approaching the theoretical storage capacity in ~5 min) and slow desorption rate (i.e., incomplete release of hydrogen in 2.5 h). Because of its slow desorption rate, the mixture can only desorb ~4.4 wt.% H_2 in each release segment. This number is clearly lower than its theoretical storage capacity which is estimated to be about 5.7 wt.% H_2 if the extra 10 mol% LiH addition and the presence of the oxides in the starting materials are considered. As a result of the un-released hydrogen at the end of each release segment, the amount of the absorbed hydrogen can only be 4.4 wt.% in each soak segment. It is also noted that little degradation in the kinetic performance occurs over the 10 soak/release cycles. This is remarkable, considering that the cyclic temperature (285 °C) is 86% of $LiNH_2$'s melting temperature and 58% of LiH's melting temperature, and that the holding time is 35 h. It is well known that holding powder compacts at high homologous temperatures (e.g., $>0.5T_m$ where T_m is the melting temperature of the material) for several hours is sufficient to cause annealing, grain growth, and even densification [20]. Thus, the unusual cyclic stability in the soak/release performance suggests that other mechanism(s) have operated to counter balance the well-known grain growth and densification effects.

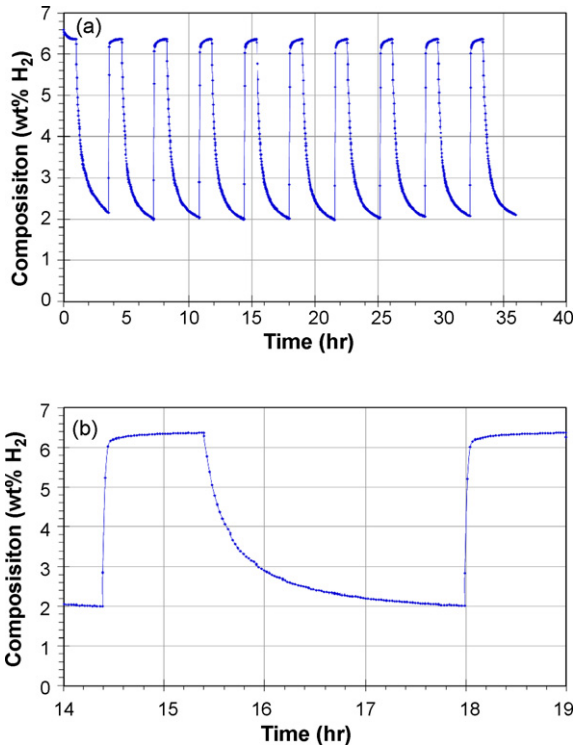

Fig. 1. Isothermal hydrogen uptake/release cycles of the $LiNH_2$ + LiH mixture at 285 °C: (a) the overall view of H_2 absorbed and desorbed as a function of cycles, and (b) the close-up of the 5th uptake/release segment.

Table 1 summarizes the crystallite sizes and SSA of the $LiNH_2$ + LiH mixture before and after isothermal soak/release cycles. Note that the crystallite sizes of LiH and $LiNH_2$ after ball milling, determined from the XRD peak broadening through the Scherrer formula [21] with the correction of instrumental broadening, are in nanoscales. Thus, it can be concluded that ball milling for 3 h has mixed LiH and $LiNH_2$ uniformly at the nanometer scale. It is further noted that the crystallite size of

Table 1
XRD-determined crystallite sizes of LiH and $LiNH_2$ and the measured specific surface area of their mixture

Sample conditions	Crystallite size of LiH (nm)	Crystallite size of $LiNH_2$ (nm)	Specific surface area of $LiH + LiNH_2$ ($m^2\ g^{-2}$)	Equivalent particle size of $LiH + LiNH_2$[a] (nm)
Before isothermal Cycling	20.8	13.3	55	51.8
After isothermal Cycling	20.0	15.9	10	284.9

[a] The equivalent particle size of the ($LiH + LiNH_2$) mixture was calculated using the specific surface area data and assuming that LiH and $LiNH_2$ had the same particle size.

LiH remains almost the same after 35 h exposure at 285 °C and 10 soak/release cycles, whereas the crystallite size of $LiNH_2$ exhibits only a slight increase. The slight or no growth of LiH and $LiNH_2$ nanocrystallites is truly remarkable, which further confirms that mechanisms opposing grain growth have been active during the isothermal soak/release cycles to maintain the nanocrystallites of LiH and $LiNH_2$, and thus offers partial explanation why the $LiNH_2$ + LiH mixture has an unusual cyclic stability in the soak/release performance. In a previous study [22], it has been established that pure LiH particles after ball milling with the identical milling condition as in this study are agglomerates of single crystals with the median crystallite size of 12 nm, which grows by 100% after the ball-milled LiH particles expose to 285 °C for 1 h in an argon atmosphere. Thus, nano-LiH particles do grow as expected, when exposed to 285 °C without soak/release cycles [22]. By comparing the behaviors of thermally exposed nano-LiH particles with and without soak/release cycling, it can be concluded that soak/release cycles do have effects on preventing nano-LiH crystallites from growing.

Note that Table 1 also shows a large decrease in the specific surface area of the $LiNH_2$ + LiH mixture after 10 isothermal soak/release cycles at 285 °C. The decrease in the SSA can only be induced by (i) crystal growth, (ii) further agglomeration of multiple particles, or (iii) both. However, the XRD analysis has revealed little or no growth of nanocrystallites. Thus, taking the SSA and crystallite size information together, it can be inferred that the ball-milled $LiNH_2$ + LiH mixture becomes further agglomerated, while their crystallite sizes remain little changed after exposing to isothermal soak/release cycles at 285 °C. Additional insights can be attained if the crystallite sizes of LiH and $LiNH_2$ determined from XRD are compared with the equivalent particle size of the $LiNH_2$ + LiH mixture calculated from the specific surface area measurement. As shown in Table 1, the equivalent particle size of the $LiNH_2$ + LiH mixture is larger than the crystallite sizes of both LiH and $LiNH_2$ before isothermal cycling, suggesting the presence of particle agglomeration. This result is in excellent agreement with previous transmission electron microscopy (TEM) analysis [22], showing agglomeration of single crystals of pure LiH particles after ball milling at the same milling condition as in this study. Table 1 also reveals that agglomeration becomes worse after isothermal cycling because of the further increased equivalent particle size of the $LiNH_2$ + LiH mixture and little or no change in the crystallite sizes of LiH and $LiNH_2$. However, it is interesting to note that the increased agglomeration does not result in obvious decreases in the soak/release performance over 10 cycles in 35 h (see Fig. 1), suggesting that the surface area is not the rate-limiting factor in the soak/release cycle at the condition employed in this study.

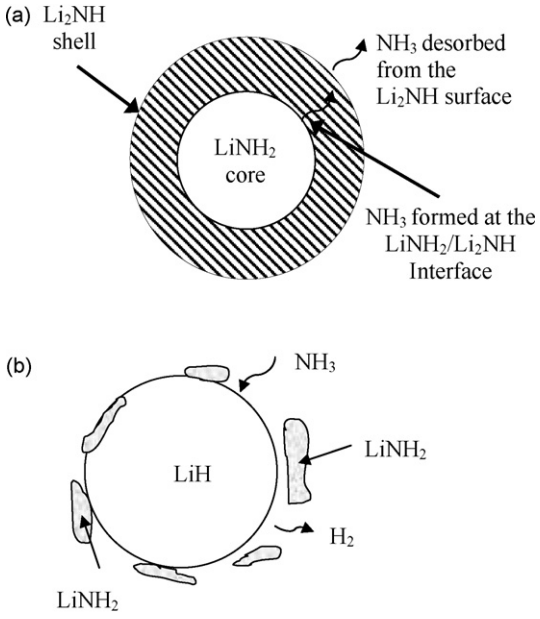

Fig. 2. Schematic of the hydrogen release pathway of the $LiNH_2$ + LiH mixture: (a) the Li_2NH product from Reaction (2) forms a continuous shell outside the $LiNH_2$ shrinking core, leading to a reaction rate controlled by NH_3 diffusion through the Li_2NH product layer, and (b) the $LiNH_2$ product from Reaction (3) flakes off continuously, resulting in direct reaction between NH_3 and constantly regenerated new LiH surface.

In order to identify the mechanism responsible for maintaining LiH and $LiNH_2$ nanocrystallites during isothermal cycling and to determine the rate-limiting step of the dehydriding reaction of the $LiNH_2$ + LiH mixture, the desorption rate in each release segment has been analyzed using various kinetic models that are possible in this system. As established in Ref. [17], the rate of Reaction (2) is controlled by diffusion of NH_3 through a porous Li_2NH product layer (Fig. 2a). Such a diffusion is necessary for continued decomposition of $LiNH_2$ at the $LiNH_2/Li_2NH$ interface and driven by the composition gradient of high NH_3 concentration at the interface and low NH_3 concentration at the free surface of Li_2NH where desorption of NH_3 takes place [17]. Note that such a conclusion, i.e., the presence of a porous Li_2NH product layer on a shrinking $LiNH_2$ core during decomposition of $LiNH_2$, is consistent with the expectation if the changes in the volumes of the solid reactant and product are examined. It is well known that the Pilling–Bedworth ratio (P–B ratio), as

shown in Eq. (4), dictates the porosity of the oxide scale and its adhesion to the metal during metal oxidation [23,24].

$$\text{P} - \text{B ratio} = \frac{V_o}{V_m} \tag{4}$$

where V_o and V_m are the volumes of the oxide scale and the metal oxidized, respectively. When the P–B ratio is less than 1, the oxide scale tends to be adherent and porous. When the P–B ratio is between 1 and 2, the oxide scale is adherent and can fully cover the metal surface although there exist compressive stresses in the scale. When the P–B ratio is large than 2, the oxide scale often cracks and flakes off because of the large compressive stress in the scale. The molar volume of $LiNH_2$ is 19.44 $cm^3\ mol^{-2}$, whereas the corresponding value for Li_2NH is 19.51 $cm^3\ mol^{-2}$. Based on the formula of Reaction (2) and the molar volumes of $LiNH_2$ and Li_2NH, the P–B ratio for Reaction (2) is found to be 0.5, thereby allowing the formation of an adherent yet porous Li_2NH product layer through which NH_3 has to diffuse and then desorb from the Li_2NH surface in order for decomposition of $LiNH_2$ to continue. When the P–B ratio of Reaction (3) is considered with the molar volume of LiH being 9.70 $cm^3\ mol^{-2}$ and the molar volume of $LiNH_2$ defined above, it is found that the P–B ratio is 2.0. Thus, the $LiNH_2$ product layer from Reaction (3), if present on the surface of the LiH core, would have extremely large compressive stresses and tend to flake off easily. Therefore, it is proposed that it is the continuous flaking off of the $LiNH_2$ product layer that constantly provides new LiH surface for reaction with NH_3 and thus Reaction (3) can proceed in the order of microseconds, as reported in Ref. [4].

The reaction pathways for Reactions (2) and (3) proposed above are shown schematically in Fig. 2. Based on the proposed reaction pathways, Reaction (2) can at least be described with the following three major steps:

$$LiNH_2 \rightarrow \frac{1}{2}Li_2NH + \frac{1}{2}NH_3\# \tag{5}$$

$$\frac{1}{2}NH_3\# \rightarrow \frac{1}{2}NH_3* \tag{6}$$

$$\frac{1}{2}NH_3* \rightarrow \frac{1}{2}NH_3 + \frac{1}{2}* \tag{7}$$

Eq. (5) represents decomposition of $LiNH_2$ to Li_2NH and NH_3 at the $LiNH_2/Li_2NH$ interface with the NH_3 absorbed at an active interfacial site, #. Eq. (6) stands for diffusion of NH_3 through the porous Li_2NH product layer from an active interfacial site, #, to an active Li_2NH surface site, * (see Fig. 2). Finally, Eq. (7) describes desorption of NH_3 from the Li_2NH surface, leaving behind an active surface site. Similarly, Reaction (3) can be described with at least three major steps:

$$\frac{1}{2}NH_3 + \frac{1}{2}\Delta \rightarrow \frac{1}{2}NH_3\Delta \tag{8}$$

$$\frac{1}{2}NH_3\Delta + \frac{1}{2}LiH \rightarrow \frac{1}{2}LiNH_2 + \frac{1}{2}H_2\Delta \tag{9}$$

$$\frac{1}{2}H_2\Delta \rightarrow \frac{1}{2}H_2 + \frac{1}{2}\Delta \tag{10}$$

Here Eq. (8) represents adsorption of NH_3 on an active LiH surface site, Δ, whereas Eq. (9) represents the absorbed NH_3 reacting with LiH to form $LiNH_2$ flakes and H_2 absorbed at an active LiH surface site, Δ. Finally, Eq. (10) describes desorption of H_2 from the LiH surface, leaving behind an active surface site.

In principle, a rate equation can be written for each major step listed above. However, experiments have established that Reaction (3) is much faster than Reaction (2) [4,17]. Thus, it can be approximated that every step in Reaction (3) is in equilibrium, while the rate of Reaction (1) is dictated by the slow step(s) of Reaction (2). Therefore, only the rate of each step in Reaction (2) needs to be investigated in order to identify the rate-limiting step of Reaction (1). This can be done by examining the fraction of H_2 released, f, as a function of holding time, t, in each release segment. If the rate of Reaction (1) is controlled by Eq. (5), the fraction of H_2 released as a function of holding time can be derived from the shrinking-core model (Fig. 2) with a $LiNH_2/Li_2NH$ interface moving at a constant speed. This relation is found to have the following format [25]:

$$(1 - f)^{1/3} = 1 - \frac{k_5}{R}t \tag{11}$$

However, if the rate of Reaction (1) is controlled by Eq. (6), then the fraction of H_2 released will follow a parabolic-rate law derived from Fick's second law [26] with the following formula [17]:

$$(1 - f)^{1/3} = 1 - \frac{k_6^{1/2}}{R}t^{1/2} \tag{12}$$

Finally, if the rate of Reaction (1) is controlled by Eq. (7), i.e., desorption of NH_3 into a chamber with a constant pressure, the fraction of H_2 released will exhibit a linear relationship between f and t [27], as shown by Eq. (13):

$$f = k_7 R^2 t \tag{13}$$

The k_5, k_6 and k_7 above are rate constants for Eqs. (11), (12) and (13), respectively, and R is the average radius of $LiNH_2$ particles.

To compare the rate Eqs. (11), (12) and (13) with the experimental data shown in Fig. 1, these rate equations need to be modified to take into account the incomplete release of H_2 at the end of each release segment. For example, Eq. (11) should be modified to

$$(1 - f'f)^{1/3} = 1 - \frac{k_5}{R}t \tag{14}$$

where f' is the fraction of H_2 released at the end of the release segment in reference to the hydrogen storage capacity of the system, which is 5.7 wt.% H_2 as discussed previously, whereas f is the fraction of H_2 released at any given time in reference to the end of the release segment. $f = 1$ at the end of each release segment, whereas $f' = 1$ only if the H_2 released at the end of the release segment equals the hydrogen storage capacity of the system. Otherwise, f' is smaller than 1. Similarly, Eqs. (12) and (13) should be modified, respectively, to be Eqs. (15) and (16).

$$(1 - f'f)^{1/3} = 1 - \frac{k_6^{1/2}}{R}t^{1/2} \tag{15}$$

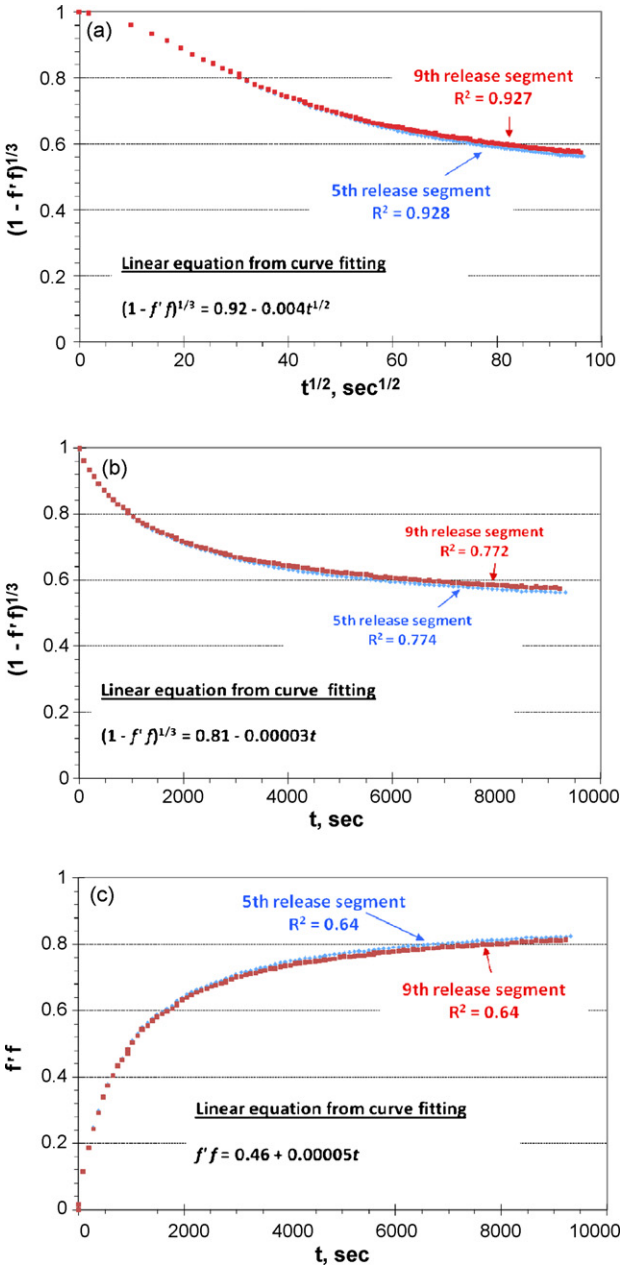

Fig. 3. The amount of H_2 released in 5th and 9th release segments shown in Fig. 1 is plotted in (a) the $(1-f'f)^{1/3}$ vs. $t^{1/2}$ fashion, as defined by Eq. (15), (b) the $(1-f'f)^{1/3}$ vs. t fashion, as defined by Eq. (14), and (c) the $f'f$ vs. t fashion, as defined by Eq. (16). Linear equations from curve fitting and the corresponding R^2 values are indicated.

$$f'f = k_7 R^2 t \tag{16}$$

Fig. 3 compares the plots of the experimental data of the 5th and 9th hydrogen release segments presented in different axes defined by Eqs. (14), (15) and (16). Clearly, the experimental data fits the diffusion-controlled model (Fig. 3a) far better than the moving-boundary-controlled (Fig. 3b) and the NH_3-desorption-controlled model (Fig. 3c) because the diffusion-controlled model has the highest R^2 value obtained from curve fitting through the least-squares method. This conclusion applies to every release segment in Fig. 1 with the 5th and 9th segments shown in Fig. 3. In spite of its highest R^2 value (Fig. 3a), the deviation of the experimental data from the linear relationship between $(1-f'f)^{1/3}$ and $t^{1/2}$ is present. This deviation is due to the gradual increase in the pressure of the sample chamber during the 15 min holding period in each evacuation step, especially at the early stage of the release segment when the diffusion distance is very short and the pressure rise is relatively quick. However, when the isothermal soak/release cycle is performed at lower temperatures and thus both the pressure rise and the diffusion rate become slower, the linearity improves substantially. Fig. 4 shows such a situation, revealing that the R^2 value almost becomes 1.0 when the isothermal soak/release cycle is conducted at 240 °C. Thus, this analysis unambiguously reveals that the rate-limiting step of Reaction (1) is diffusion of NH_3 through the porous Li_2NH product layer.

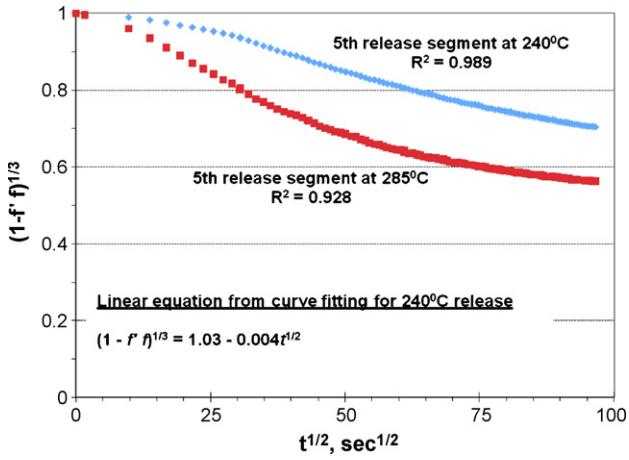

Fig. 4. A comparison of the amounts of H_2 released as a function of time in the 5th release segments of the isothermal soak/release cycles at 240 and 285 °C, plotted in the $(1-f'f)^{1/3}$ vs. $t^{1/2}$ fashion, as defined by Eq. (15).

4. Concluding remarks

The present set of experiments reveals that nanocrystalline LiH and $LiNH_2$ particles generated via high-energy ball milling exhibit little or no growth in nanocrystallite sizes after 10 hydrogen soak/release cycles at 285 °C for 35 h. However, the surface area of the $LiNH_2$ + LiH powder mixture does decrease, indicating an increase in particle agglomeration during isothermal cycling. Nevertheless, the isothermal hydrogen soak/release performance exhibits little or no degradation. The unusual cyclic stability of the nanocrystalline $LiNH_2$ + LiH mixture has been attributed to (i) repeated nucleation of solid phases during hydriding and dehydriding reactions and (ii) the continuous flaking off of the $LiNH_2$ product layer from the surface of the LiH reactant. The latter, in conjunction with the presence of H_2 gas, effectively prevents substantial decrease in the specific surface area and densification during isothermal cycling for 35 h at very high homologous temperatures (i.e., 86% of $LiNH_2$'s melting temperature and 58% of LiH's melting temperature). Dehydrogenation of the $LiNH_2$ + LiH mixture is found to be diffusion-controlled and the rate-limiting step is identified to be diffusion of NH_3 through the porous Li_2NH product layer out-

side the $LiNH_2$ shrinking core. A reaction pathway has been proposed to explain ultrafast reaction between LiH and NH_3 as well as slow decomposition of $LiNH_2$ to Li_2NH and NH_3. The model proposed is in good agreement with experimental observations including (i) the change in the volume of the solid before and after reactions, (ii) the limited increase in particle agglomeration over 35 h at very high homologous temperatures, and (iii) the substantially different reaction rates between Reactions (2) and (3) although both reactions generate solid and gaseous products.

Acknowledgements

This work was supported under the US Department of Energy (DOE) Contract no. DE-FC36-05GO15008. The vision and support of Drs. Carole J. Read and Ned T. Stetson, DOE Technology Managers, are greatly appreciated.

References

[1] P. Chen, Z. Xiong, J.Z. Luo, J.Y. Lin, K.L. Tan, Interaction of hydrogen with metal nitrides and imides, Nature 420 (2002) 302–304.
[2] P. Chen, Z. Xiong, J.Z. Luo, J.Y. Lin, K.L. Tan, Interaction between lithium amide and lithium hydride, J. Phys. Chem. B 107 (2003) 10967–10970.
[3] Y.H. Hu, E. Ruckenstein, H_2 storage in Li_3N. Temperature-programmed hydrogenation and dehydrogenation, Ind. Eng. Chem. Res. 42 (2003) 5135–5139.
[4] Y.H. Hu, E. Ruckenstein, Ultrafast reaction between LiH and NH_3 during H_2 storage in Li_3N, J. Phys. Chem. A 107 (2003) 9737–9739.
[5] T. Ichikawa, N. Hanada, S. Isobe, H. Leng, H. Fujii, Mechanism of novel reaction from $LiNH_2$ and LiH to Li_2NH and H_2 as a promising hydrogen storage system, J. Phys. Chem. B 108 (2004) 7887–7892.
[6] T. Ichikawa, S. Isobe, N. Hanada, H. Fujii, Lithium nitride for reversible hydrogen storage, J. Alloys Compd. 365 (2004) 271–276.
[7] S. Orimo, Y. Nakamori, G. Kitahara, K. Miwa, N. Ohba, T. Noritake, S. Towata, Destablization and enhanced dehydriding reaction of $LiNH_2$: an electronic structure viewpoint, Appl. Phys. A 79 (2004) 1765–1767.
[8] T. Ichikawa, N. Hanada, S. Isobe, H. Leng, H. Fujii, Composite materials based on light elements for hydrogen storage, Mater. Trans. 46 (2005) 1–14.
[9] Y. Kojima, Y. Kawai, IR characterization of lithium imide and amide, J. Alloys Compd. 395 (2005) 236–239.
[10] Y.H. Hu, E. Ruckenstein, Highly effective Li_2O/Li_3N with ultrafast kinetics for H_2 storage, Ind. Eng. Chem. Res. 43 (2004) 2464–2467.
[11] J.H. Yao, C. Shang, K.F. Aguey-Zinsou, Z.X. Guo, Desorption characteristics of mechanically and chemically modified $LiNH_2$ and ($LiNH_2$ + LiH), J. Alloys Compd. 432 (2007) 277–282.
[12] H.Y. Leng, T. Ichikawa, S. Isobe, S. Hino, N. Hanada, H. Fujii, Desorption behaviors from metal-N-H systems synthesized by ball milling, J. Alloys Compd. 404–406 (2005) 443–447.
[13] G.P. Meisner, F.E. Pinkerton, M.S. Meyer, M.P. Balogh, M.D. Kundrat, Study of the lithium–nitrogen–hydrogen system, J. Alloys Compd. 404–406 (2005) 24–26.
[14] S. Isobe, T. Ichikawa, N. Hanada, H.Y. Leng, M. Fichtner, O. Fuhr, H. Fujii, Effect of Ti catalyst with different chemical form on Li–N–H hydrogen storage properties, J. Alloys Compd. 404–406 (2005) 439–442.
[15] T. Ichikawa, N. Hanada, S. Isobe, H.Y. Leng, H. Fujii, Hydrogen storage properties in Ti catalyzed Li–N–H systems, J. Alloys Compd. 404–406 (2005) 435–438.
[16] L. Shaw, R. Ren, T. Markmaitree, W. Osborn, Effects of mechanical activation on dehydrogenation of the lithium amide and hydride system, J. Alloys Compd. 448 (2008) 263–271.
[17] T. Markmaitree, R. Ren, L. Shaw, Enhancement of lithium amide to lithium imide transition via mechanical activation, J. Phys. Chem. B 110 (2006) 20710–20718.
[18] Z.-G. Yang, L. Shaw, Synthesis of nanocrystalline SiC at ambient temperature through high energy reaction milling, Nanostruct. Mater. 7 (1996) 873–886.
[19] S. Brunauer, P.H. Emmett, E. Teller, Adsorption of gases in multimolecular layers, J. Am. Chem. Soc. 60 (1938) 309–319.
[20] R.M. German, Powder Metallurgy Science, Metal Powder Industries Federation, Princeton, New Jersey, USA, 1994.
[21] H.P. Klug, L.E. Alexander, X-ray Diffraction Procedures for Polycrystalline and Amorphous Materials, John Wiley & Sons Inc., London, 1954.
[22] A.L. Ortiz, W. Osborn, T. Markmaitree, L. Shaw, Crystallite sizes of LiH before and after ball milling and thermal exposure, J. Alloys Compd., available on line: doi:10.1016/j.jallcom.2006.12.035, in press.
[23] N.B. Pilling, R.E. Bedworth, The oxidation of metals at high temperature, J. Inst. Met. 29 (1923) 529.
[24] H. Rode, D. Orlicki, V. Hlavacek, Noncatalytic gas–solid reactions and mechanical stress generation, AIChE J. 41 (1995) 1235.
[25] L.N. Dinh, C.M. Cecala, J.H. Leckey, M. Balooch, The effects of moisture on LiD single crystals studied by temperature-programmed decomposition, J. Nucl. Mater. 295 (2001) 193.
[26] P.G. Shewmon, Diffusion in Solid, J. Williams Book Company, Jenks, OK, USA, 1983.
[27] J.M. Thomas, W.J. Thomas, Principles and Practice of Heterogeneous Catalysis, VCH, Weinheim, Germany, 1997.